Batteries & Supercaps

Research Article
doi.org/10.1002/batt.202400046

Chemistry Europe
European Chemical Societies Publishing

www.batteries-supercaps.org

$V_2O_5 \cdot nH_2O$ and Graphene Oxide/CNTs Composite Film as Binder-Free Cathode for Aqueous Zinc-Ion Batteries

Diwen Rao,[a, b] Wenwei Zhang,[a] Baochen Cheng,[c] Yu Wang,[a] Chengsifan Lei,[a, b] Qinyou An,[a, b] Meng Huang,*[b] and Liqiang Mai*[a, b]

Emerging as a leading contender for economical, high-security grid-scale energy storage, rechargeable aqueous zinc-ion batteries (AZIBs) are currently facing the challenge in its progression due to the absence of cathode materials with high energy density. In this study, we design a $V_2O_5 \cdot nH_2O$, GO and CNTs composite (HVO/GO-CNTs) film through freeze-drying and vacuum filtration. This binder-free cathode for AZIBs exhibits remarkable electrochemical performance, featuring a high capacity of 387 $mAh\,g^{-1}$ at 0.2 $A\,g^{-1}$ and a high capacity retention of 82.6% after 1000 cycles at 1 $A\,g^{-1}$. This investigation offers a promising approach to electrode material design for the advancement of high-performance AZIBs.

Introduction

For centries, fossil energies have been heavily overused and caused serious environmental damages, on account of greenhouse gases, including sulfides, nitrides and carbon dioxides etc. released during combustion and use, and importantly, they have limited reserves.[1,2] Therefore, there has been a surge in research towards the development of renewable energy sources aiming to minimize the usage of fossil fuels.[3] Electrochemical energy storage technology developed for large-scale renewable energy is supposed to be high conversion efficiency, low price, simple maintenance and miniaturization.[4] In recent decades, rechargeable aqueous zinc-ion batteries (AZIBs) have been proposed as a promising candidate for economical and high-safety grid-scale energy storage. As an abundant, inexpensive, and non-toxic metal, zinc possesses attractive attributes such as high theoretical capacity, low redox potential, high safety and sustainability, making it a promising anode material.[5,6] Furthermore, the use of aqueous electrolytes in AZIBs brings added advantages, mainly due to their inherent safety, high ionic conductivity, and cost-effectiveness.

Despite these attractive properties, significant challenges remain to be resolved in the development of AZIBs, particularly on the cathode side. To date, extensive researches have been conducted on manganese oxides, Prussian blue and its analogues, polyanionic compounds, and vanadium-based materials as AZIBs cathode materials.[7] Among these, vanadium-based materials have received considerable attention due to their multivalence, naturally abundant reserves, and low cost, primarily focusing on layered vanadium oxide and vanadates. Vanadium pentoxides (V_2O_5) are a commonly used cathode in lithium-ion and sodium-ion batteries.[8-10] Due to their adjustable layered structure and various redox states of vanadium, they have also been widely studied as a promising ZIB cathode. However, for Zn^{2+}, the interlayer distance in the original V_2O_5 framework is actually limited, which spatially hinders ion diffusion dynamics and ultimately leads to rapid performance degradation in long-term cycling.[11] However, Zn^{2+} can also coordinate with water molecules in aqueous solutions to form hydrated ions with a size of ≈5.5 Å, which will definitely bring additional difficulties to the insertion and extraction of zinc ions.[12] To promote the kinetics process, an effective approach is to introduce embedded objects, such as Li^+, Na^+, Ca^{2+}, and Mg^{2+} to expand interlayer spacing, thereby improving rate and cycling performance.[13–15] Moreover, the hydrated double-layer V_2O_5 ($V_2O_5 \cdot nH_2O$, HVO) has recently attracted much attention, in which the pillar-like water molecules expand the interlayer spacing.[16,17] In comparison to the piller-like metal ions, water molecules can simultaneously act as a charge shield for zinc ions, partially reducing their interaction with the host sublattice oxygen.[18–20] However, repeated insertion and extraction of Zn^{2+} still inevitably lead to structural degradation of the main material. In addition, intrinsic poor electronic conductivity of HVO also limits the reaction kinetics.[21]

Thereafter, one-stone-two-birds method is of great interests to build high-performance HVO cathode.[22] Graphene oxide (GO), renowned for its two-dimensional layered structure, has high electronic conductivity, mechanical strength, and surface area, and thus is widely used to improve the electrochemical performance of the electrodes.[23,24] Carbon Nanotubes (CNTs)

[a] D. Rao, W. Zhang, Y. Wang, C. Lei, Prof. Q. An, Prof. L. Mai
State Key Laboratory of Advanced Technology for Materials Synthesis and Processing,
School of Materials Science and Engineering
Wuhan University of Technology
122 Luoshi Road, 430070 Wuhan (China)
E-mail: mlq518@whut.edu.cn

[b] D. Rao, C. Lei, Prof. Q. An, Dr. M. Huang, Prof. L. Mai
Sanya Science and Education Innovation Park of Wuhan University of Technology
Sanya 572000, China
E-mail: 211808@whut.edu.cn

[c] Dr. B. Cheng
State Key Laboratory of Maritime Technology and Safety,
School of Navigation
Wuhan University of Technology
1178 Heping Avenu, 430063 Wuhan (China)

Supporting information for this article is available on the WWW under https://doi.org/10.1002/batt.202400046

Research Article
doi.org/10.1002/batt.202400046
Chemistry Europe
European Chemical Societies Publishing

featuring excellent mechanical strength, conductivity, chemical stability, and large surface area, are widely used.[25,26] Thus, the integrating GO and CNTs with materials is a promising methode to address some of the aforementioned issues.[27]

In this work, HVO are compounded with GO and CNTs (HVO/GO-CNTs) by freeze-drying and vacuum filtration to improve the cycling stability and electronic conductivity of the cathode. The obtained HVO/GO-CNTs binder-free film of high flexibility and mechanical strength can be directly used as an electrode. As a result, HVO/GO-CNTs film showcases an exceptional specific capacity of 387 mAh g^{-1} at the current density of 0.2 A g^{-1}. At 1.0 A g^{-1}, the capacity can be maintained at 316 mAh g^{-1}, and after 1000 cycles, it can still deliver 261 mAh g^{-1}, suggesting a high-rate capability and stable cyclability of HVO/GO-CNTs film.

Results and Discussion

Due to the mutual repulsion between layers, graphene oxides (GO) has good dispersion in aqueous solution and excellent compatibility with carbon nanotubes (CNTs). CNTs and rGO have excellent conductivity and can effectively improve electrochemical performance. Moreover, due to the presence of -OH, -CHO, -COOH, etc., the GO film exhibits high hydrophilicity.[28,29] Therefore, HVO, GO and CNTs were first dispersed in aqueous solution, and then a composite film (HVO/GO-CNTs) was obtained through vacuum filtration. The binder-free hybrid composite film facilitates and saves time in assembling batteries, and is supposed to have high performance for AZIBs.

X-ray diffraction (XRD) examination was performed to examine the composition of the final film, and the comparison between HVO/GO-CNTs and HVO is shown in Figure 1a. The (001) peak located at 2θ of 7.18° suggests that these materials have a large interlayer distance of 1.23 nm owing to the intercalated water molecules.[30] Meanwhile, Fourier transform infrared (FTIR) spectra were also collected to characterize chemical bonds and functional groups (Figure 1b). The peak at 3540 cm^{-1} is the bending vibration of the O–H bond in H_2O. The peak at 1627 cm^{-1} is attributed to the vibration of COOH. The peak near 993 cm^{-1} represents the stretching vibration of $V^{5+}=O$. The stretching vibrations, both symmetric and asymmetric of V–O–V are reflected at 734 cm^{-1} and 449 cm^{-1}, respectively. The overall results suggest the presence of $V_2O_5{\cdot}nH_2O$.[31]

The morphology of the HVO/GO-CNTs film was studied using scanning electron microscopy (SEM) and transmission electron microscopy (TEM). In Figure 1c, it can be seen that the the HVO/GO-CNTs film has a smooth surface. Figure 1d shows that the film has a multi-layer structure. The microstructure of the thin film can be seen in Supplementary Figure S1a and S1b. Figure 1e shows a SEM image of a cross-section of the film,

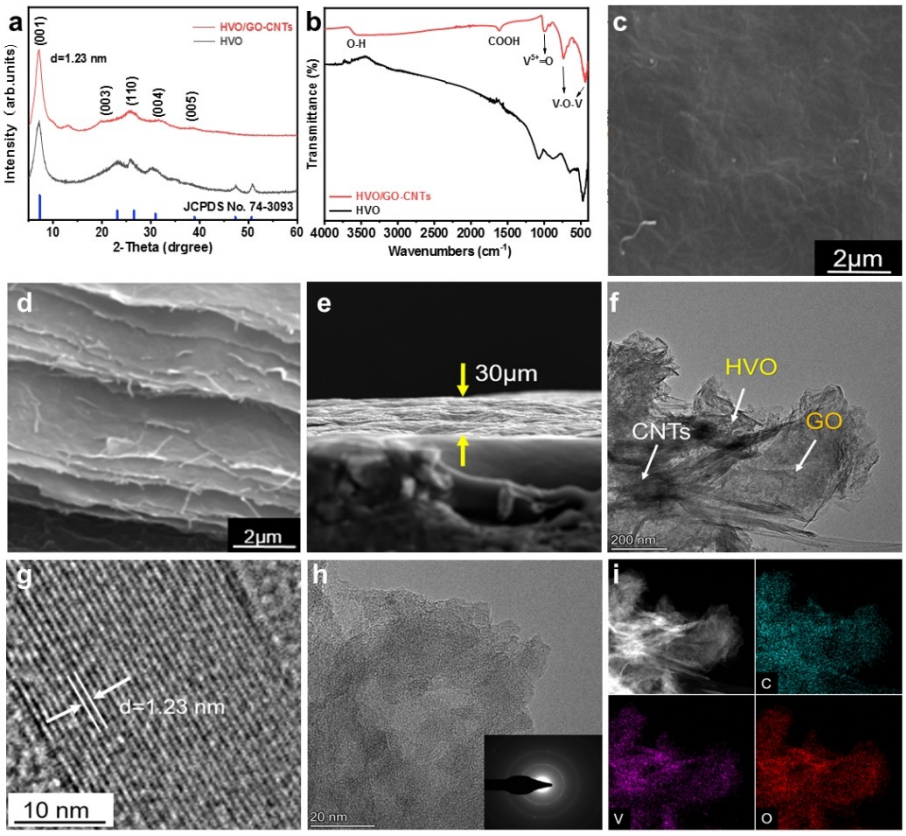

Figure 1. (a) XRD patterns and (b) FTIR spectra of HVO and HVO/GO-CNTs. (c-e) SEM images, (f) TEM image, (g) HRTEM image, (h) SAED pattern and (i) elemental mappings of HVO/GO-CNTs.

Research Article
doi.org/10.1002/batt.202400046
Chemistry Europe
European Chemical Societies Publishing

showing a thickness of approximately 30 μm. HVO has a sheet-like morphology with a size of about a few micrometers (Figure S1c), which is different from V_2O_5 nanoparticles (Figure S1d). High resolution TEM (HRTEM) shows that HVO/GO-CNTs have a clear lattice structure with an interlayer spacing of 1.23 nm (Figure 1g), which is consistent with the XRD result. Therefore, HVO/GO-CNTs has a large interlayer spacing and can provide smooth diffusion path for ions. Figure 1f shows that HVO, GO and CNTs are well crosslinked in the film. The selected area electron diffraction of Figure 1h proves that the HVO/GO-CNTs film is polycrystalline. Energy dispersive X-ray spectroscopy (EDS) spectra (Figure 1i) shows that C, O, and V elements are uniformly distributed in HVO/GO-CNTs. In addition, strong D and G peaks can be observed in Raman spectroscopy (Figure S2), which proves the good combination of GO and CNTs. The value of I_D/I_G of HVO/GO-CNTs film is calculated as 1.0, which means that the carbon material has low defects and thus high electronic conductivity. The intercalated water content of the sample determined by thermogravimetric analysis (TGA) is approximately 10 wt% (Figure S3).

The electrochemical performances of HVO and HVO/GO-CNTs film as cathodes for AZIBs were investigated. The 3 M zinc trifluoromethanesulfonate ($Zn(CF_3SO_3)_2$) aqueous solution and zinc plate are used as the electrolyte and anode, respectively. To confirm these two materials' ability to store energy, a galvanostatic charge-discharge (GCD) comparison was conducted between HVO and HVO/GO-CNTs film. The GCD tests at 0.2 A g^{-1} (Figure 2a) show that HVO and HVO/GO-CNTs have similar initial discharge capacity (approximately 387 mAh g^{-1}). However, after 100 cycles of charging and discharging, the capacity of HVO/GO-CNTs film still maintains at 298 mAh g^{-1}, while that of HVO only maintains at 206 mAh g^{-1}, indicating excellent cycling stability of the HVO/GO-CNTs film. HVO/GO-CNTs show two pairs of redox plateaus, and the plateaus show slow degradation upon cycling (Figure 2b). In the rate test, the HVO/GO-CNTs film exhibits discharge specific capacities of 380, 348, 305, and 250 mAh g^{-1} at 0.2, 0.5, 1, and 2 A g^{-1}, respectively. In contrast, HVO exhibits capacities of 302, 269, 228, and 180 mAh g^{-1} at the corresponding current densities (Figure 2c). This indicates that HVO/GO-CNTs film has better rate capability than HVO. Figure 2d shows the constant current discharging/charging curves of HVO/GO-CNTs film at different current densities. It is worth noting that at a high current rate of 2 A g^{-1}, the discharge plateaus are still visible. In addition, HVO/GO-CNTs film has an excellent long-term cycling stability, with a much higher capacity retention of 82.6% than that of HVO (22.6%) at 1 A g^{-1} after 1000 cycles (Figure 2e). This result indicates that GO and CNTs have positive effects on the ion storage kinetics and structure stability of HVO during long-term cycling. In addition, the cycling stability of HVO/GO cathode without the addition of CNTs at 200 mA g^{-1} is significantly reduced (Figure S4), which further supports that the positive effects of GO film on the structure stability of HVO. Figure S5 presents electrochemical impedance spectroscopy (EIS) results of HVO and HVO/GO-CNTs. It is obvious that the HVO/GO-CNTs electrode has much smaller charge transfer resistances, demonstrating the superior electronic conductivity of HVO/GO-CNTs.[32]

To delve deeper into the reaction kinetics, data from CV tests between 0.2 and 1.6 V at various scanning rates (0.1 to 0.6 mV s^{-1}) were analyzed (Figure 3a). During the energy storage process, the CV curves unambiguously show two redox reactions, represented by two pairs of clear redox peaks. These observations are in line with the GCD curves. As the scanning rate increases, voltage polarization increases due to the ohmic resistance. Based on the trend of redox peak changes, the

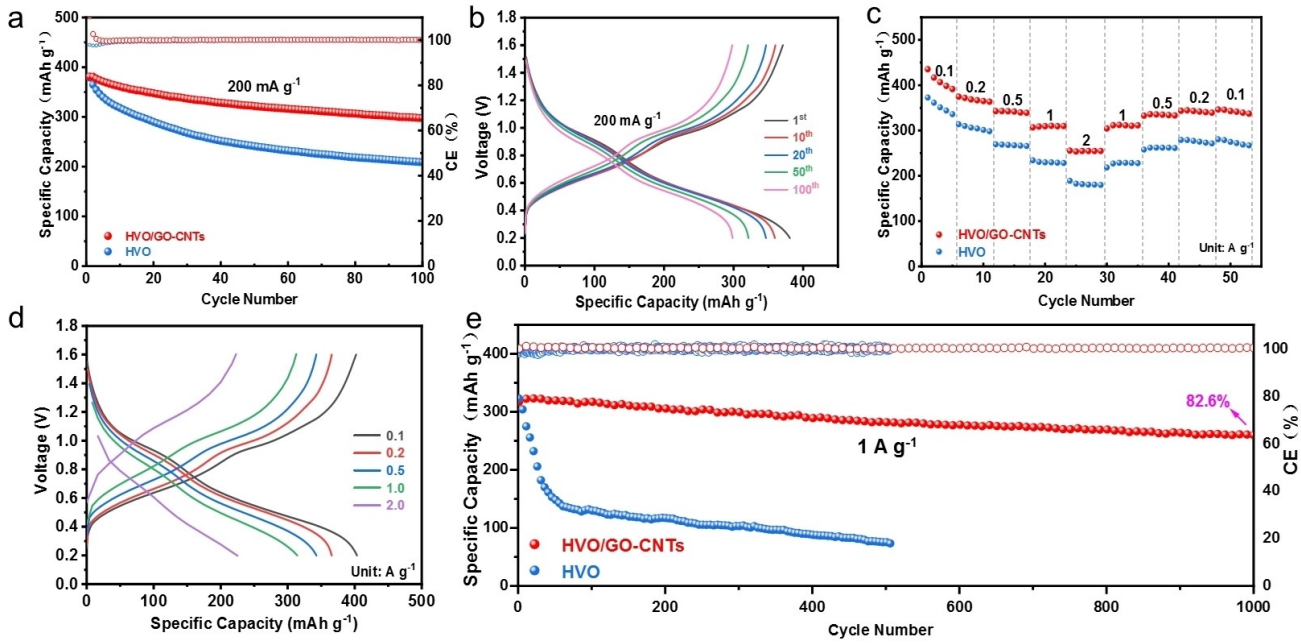

Figure 2. (a) Cycling performance at 200 mA g^{-1} of HVO/GO-CNTs and HVO. (b) Charge–discharge curves of HVO/GO-CNTs at 200 mA g^{-1}. (c) Rate performance of HVO/GO-CNTs and HVO. (d) GCD profiles at various current densities of HVO/GO-CNTs. (e) Cycling performance of HVO/GO-CNTs and HVO at 1 A g^{-1}.

Research Article
doi.org/10.1002/batt.202400046
Chemistry Europe
European Chemical Societies Publishing

following formulas can be used to examine the reaction kinetics:

$$i = av^b \quad (1)$$

$$\log i = b\log v + \log a \quad (2)$$

In the equation above, i is the current (mA), v is the sweep rate ($mV\,s^{-1}$) of the redox peak, and a and b are constants. If b equals 0.5, diffusion process completely controls the reaction. However, when b equals 1, non-diffusion factors completely govern the reaction. The b values gleaned from fitting the four peaks are 0.84, 0.87, 0.75, and 0.84, respectively (Figure 3b), highlighting the dominance of non-diffusion energy storage process in the HVO/GO-CNTs film. Due to the fact that the energy storage process is determined by both diffusion and non-diffusion factors, the contribution rate can be calculated using equation (3):

$$i(V) = k_1 v + k_2 v^{1/2} \quad (3)$$

In the equation (3), k1 and k2 are constants at a defined scanning rate.[33] The capacitive contribution, represented by the shaded area (Figure 3c), is 75% at the scanning rate of $0.6\,mV\,s^{-1}$. The capacitive contribution increase from 61% to 66%, 71%, and 75% as the scanning rate increase from 0.1 to 0.2, 0.4, and $0.6\,mV\,s^{-1}$ (Figure 3d), which indicates that the specific capacity of HVO/GO-CNTs film is mainly controlled by non-diffusion factor. As the scanning rate increases, the contribution of capacitive behavior becomes more dominated. The diffusion coefficients of Zn^{2+} in AZIB can be calculated using the Randles-Sercik formula as follows:

$$D = \left(\frac{I_p}{2.69 \times 10^5 n^{3/2} A C v^{1/2}}\right)^2 \quad (4)$$

Where A is the cathode area (cm^2), C is the ion concentration (mol cm^{-3}), v is the scanning rate ($V\,s^{-1}$), I_p is the peak current (A), and n is the number of electron transfers during the redox process. The ion diffusion coefficients are calculated to be 7.36×10^{-10}, 6.53×10^{-10}, 4.88×10^{-10} and 3.58×10^{-10} $cm^2\,s^{-1}$ for peak 1, 2, 3, and 4, respectively (Figs 3 e, f), revealing that the HVO/GO-CNTs has good ion diffusion kinetics. In contrast, the ion diffusion coefficients of HVO are only about half that of HVO/GO-CNTs (Figs 3 g-i).

Ex-situ XRD and XPS analyses were performed to investigate the energy storage process (Figure 4). When discharged to 0.7 V, the intensity of the main peak at $2\theta = 7.1°$ significantly decreases (Figure 4a), indicating that zinc ions are intercalated and stored in the layered structure of $V_2O_5 \cdot nH_2O$. Two peaks at 12.5° and 20.9° are well related to the zinc pyrovanadate phase ($Zn_3V_2O_7(OH)_2 \cdot nH_2O$, PDF 01–087-0417, ZVO), which is formed

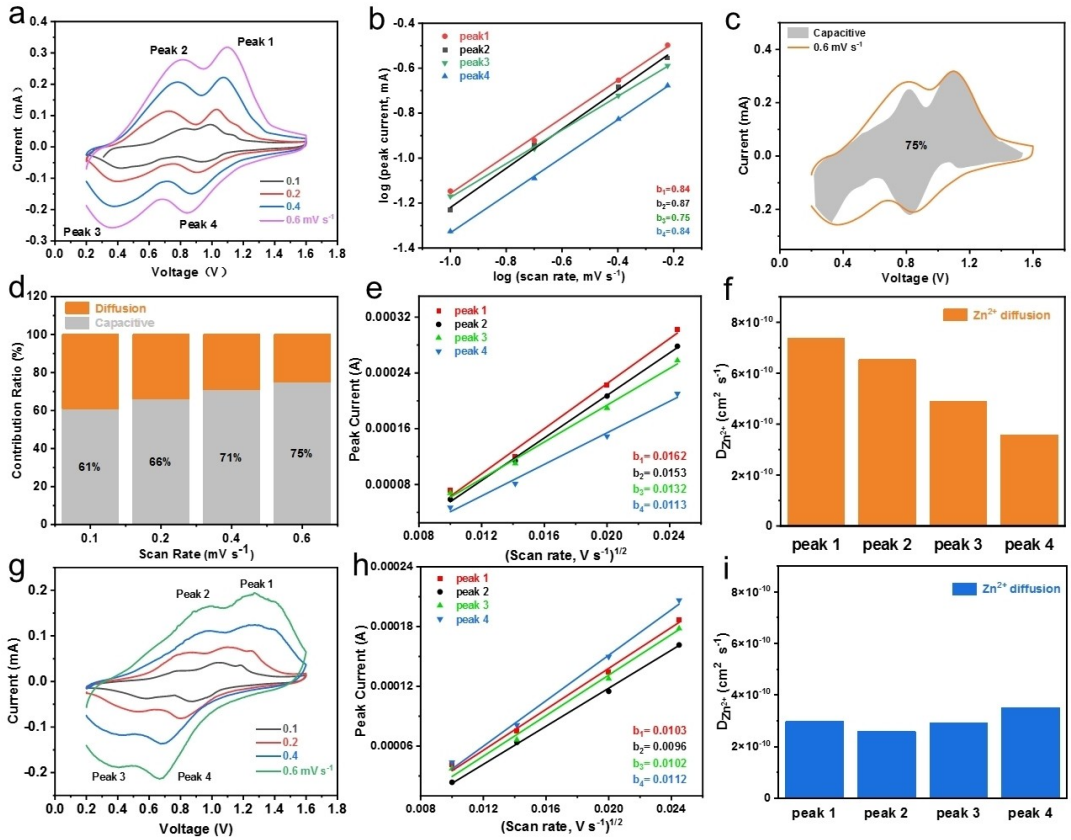

Figure 3. (a) CV curves of HVO/GO-CNTs at 0.1~0.6 $mV\,s^{-1}$. (b) The relationship between log (scan rate) and log (peak current). (c) CV curve with capacity separation at 0.6 $mV\,s^{-1}$. (d) Capacitive contributions at different scan rate. (e) The relationship between $(scan\ rate)^{1/2}$ and peak current. (f) Zn^{2+} diffusion at peak current. (g) CV curves of HVO at 0.1~0.6 $mV\,s^{-1}$. (h) The relationship between $(scan\ rate)^{1/2}$ and peak current. (i) Zn^{2+} diffusion at peak current.

Research Article
doi.org/10.1002/batt.202400046
Chemistry Europe
European Chemical Societies Publishing

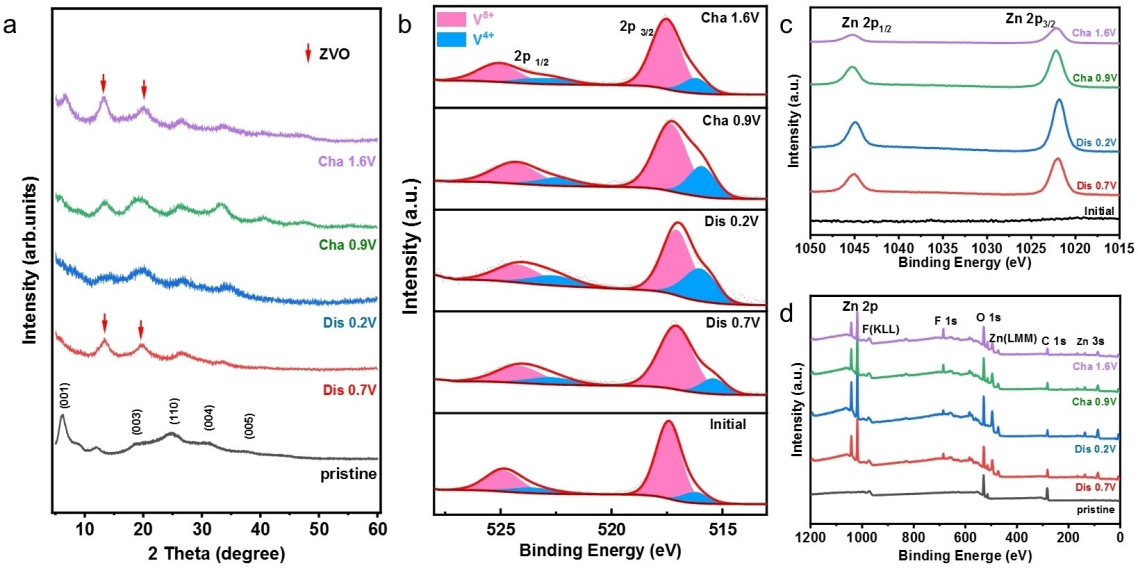

Figure 4. (a) XRD patterns and (b) XPS spectra of HVO/GO-CNTs at different discharged/charged states. (c) Zn 2p at different discharged/charged states. (d) Ex-situ high-resolution XPS spectra.

during the discharge process.[34] Following a discharge to 0.2 V, the primary peak located at 7.1° vanishes entirely. The primary peak at 7.1°, which represents the extraction of zinc ions, starts to show after the battery is recharged to 0.9 V. Ultimately, the major peak at 7.1° is recovered when the battery is charged to 1.6 V, and the peaks at 12.5° and 20.9° are ascribed to residual ZVO. The ratio of V^{4+} sharply rises and the ratio of V^{5+} correspondingly falls when the cathode discharges from its initial state to 0.2 V, suggesting that the insertion and adsorption of Zn^{2+} lower the valence state of V (Figure 4b). Ultimately, V^{5+} is recovered, demonstrating its exceptional reversibility, during the subsequent charging procedure.[35] The cathode has no signal of Zn^{2+} at its initial state (Figure 4c). After discharging to 0.2 V, two strong and sharp peaks at 1022 eV and 1045 eV, corresponding to Zn $2p_{3/2}$ and $2p_{1/2}$, respectively, are observed, which are caused by the insertion of Zn^{2+}. The weak Zn^{2+} peak at fully charged cathode is attributed to the partial irreversible intercalation of Zn^{2+}. In the survey spectra, the observed F 1s peak is derived from the residual trifluoromethanesulfonic acid ions on the electrode surface (Figure 4d).

Conclusions

In summation, we have engineered an innovative approach for creating a binder-free HVO/GO-CNTs film through the freeze-drying and vacuum filtration as cathode for AZIBs. The HVO/GO-CNTs film exhibits a specific capacity of 387 mAh g^{-1} at a current density of 0.2 A g^{-1}, and 316 mAh g^{-1} at 1.0 A g^{-1}, 82.6% of which maintains after 1000 cycles. In addition, ex-situ testing reveals fast diffusion-controlled energy storage processes. This research provides a simple and effective method of designing high-performance cathode for AZIBs.

Materials & Methods

The HVO was meticulously fabricated using a sol-gel process devoid of thermal treatment (Figure S6). In the initial stages, 0.3 g V_2O_5 was dispersed into deionized water (5 ml) and 1.5 ml 30 wt% hydrogen peroxide solution was added. The mixture was stabilized through a 15 minute stirring session, followed by the incorporation of 20 ml deionized water. The uniform dark red solution was then subjected to a 2-hour ultrasonication process and subsequently freeze dried for 48 hours to obtain the HVO gel.

To prepare the film, HVO (14 mg), graphene oxide (GO, 4 mg), and carbon nanotubes (CNTs, 2 mg) were dispersed in deionized water (15 ml). The mixture is stirred vigorously for 6 hours and then dispersed by sonication for 2 hours. After vigorous agitation, the suspension was directed to a filtration setup where it was suction filtered with a polyethersulfone membrane. After a natural drying (25 °C) phase of 24 hours, the self-standing HVO/GO-CNTs film was carefully stripped off. Subsequently, it can be cut to a suitable size for direct use as electrode sheets.

A more comprehensive explanation is provided in the Supporting Information.

Acknowledgements

This work was supported by the National Natural Science Foundation of China (52172231, 52172233 and 51972259), the Sanya Science and Education Innovation Park of Wuhan University of Technology (2022KF0011), and the Natural Science Foundation of Hubei Province (2022CFA087).

Conflict of Interests

The authors declare no conflict of interest.

Data Availability Statement

The data that support the findings of this study are available from the corresponding author upon reasonable request.

Keywords: Vanadium pentoxide · Zinc ion battery · Binder-free cathode · Carbon material

[1] X. D. Li, S. M. Wang, L. Li, X. L. Zu, Y. F. Sun, Y. Xie, *Acc. Chem. Res.* **2020**, *53*, 2964–2974.
[2] M. Ismael, *J. Alloys Compd.* **2020**, *846*, 156446.
[3] Y. B. Li, J. Fu, C. Zhong, T. P. Wu, Z. W. Chen, W. B. Hu, K. Amine, J. Lu, *Adv. Energy Mater.* **2019**, *9*, 1802605.
[4] P. Poizot, J. Gaubicher, S. Renault, L. Dubois, Y. L. Liang, Y. Yao, *Chem. Rev.* **2020**, *120*, 6490–6557.
[5] X. X. Jia, C. F. Liu, Z. G. Neale, J. H. Yang, G. Z. Cao, *Chem. Rev.* **2020**, *120*, 7795–7866.
[6] G. Z. Fang, J. Zhou, A. Q. Pan, S. Q. Liang, *ACS Energy Lett.* **2018**, *3*, 2480–2501.
[7] L. Chen, Q. An, L. Mai, *Adv. Mater. Interfaces* **2019**, *6*, 1900387.
[8] Y. Ding, L. Zhang, X. Wang, L. Han, W. Zhang, C. Guo, *Chin. Chem. Lett.* **2023**, *34*, 107399.
[9] Y. J. Zhang, X. Y. Yuan, T. Lu, Z. W. Gong, L. K. Pan, S. W. Guo, *J. Colloid Interface Sci.* **2021**, *585*, 347–354.
[10] D. McNulty, D. N. Buckley, C. O'Dwyer, *ACS Appl. Energ. Mater.* **2019**, *2*, 822–832.
[11] N. Liu, B. Li, Z. He, L. Dai, H. Wang, L. Wang, *J. Energy Chem.* **2021**, *59*, 134–159.
[12] J. P. Yan, E. H. Ang, Y. Yang, Y. F. Zhang, M. H. Ye, W. C. Du, C. C. Li, *Adv. Funct. Mater.* **2021**, *31*, 2010213.
[13] C. Xia, J. Guo, P. Li, X. X. Zhang, H. N. Alshareef, *Angew. Chem. Int. Ed.* **2018**, *57*, 3943–3948.
[14] B. W. Lin, X. H. Zhu, L. Z. Fang, X. Y. Liu, S. Li, T. Zhai, L. Xue, Q. B. Guo, J. Xu, H. Xia, *Adv. Mater.* **2019**, *31*, 1900060.
[15] H. Geng, M. Cheng, B. Wang, Y. Yang, Y. Zhang, C. C. Li, *Adv. Funct. Mater.* **2019**, *30*, 1907684.
[16] P. Hu, P. Hu, T. D. Vu, M. Li, S. C. Wang, Y. J. Ke, X. T. Zeng, L. Q. Mai, Y. Long, *Chem. Rev.* **2023**, *123*, 4353–4415.
[17] G. Z. Yang, T. Y. Wei, C. X. Wang, *ACS Appl. Mater. Interfaces.* **2018**, *10*, 35079–35089.
[18] S. Liu, L. Kang, J. M. Kim, Y. T. Chun, J. Zhang, S. C. Jun, *Adv. Energy Mater.* **2020**, *10*, 2000477.
[19] Y. Liu, X. Wu, *J. Energy Chem.* **2021**, *56*, 223–237.
[20] M. Yan, P. He, Y. Chen, S. Wang, Q. Wei, K. Zhao, X. Xu, Q. An, Y. Shuang, Y. Shao, K. T. Mueller, L. Mai, J. Liu, J. Yang, *Adv. Mater.* **2018**, *30*, 1703725.
[21] J. Cao, D. D. Zhang, X. Y. Zhang, Z. Y. Zeng, J. Q. Qin, Y. H. Huang, *Energy Environ. Sci.* **2022**, *15*, 499–528.
[22] D. D. Zhang, J. Cao, Y. L. Yue, T. Pakornchote, T. Bovornratanaraks, J. T. Han, X. Y. Zhang, J. Q. Qin, Y. H. Huang, *ACS Appl. Mater. Interfaces.* **2021**, *13*, 38416–38424.
[23] Y. V. M. Reddy, J. H. Shin, V. N. Palakollu, B. Sravani, C. H. Choi, K. Park, S. K. Kim, G. Madhavi, J. P. Park, N. P. Shetti, *Adv. Colloid Interface Sci.* **2022**, *304*, 102664.
[24] F. Farjadian, S. Abbaspour, M. A. A. Sadatlu, S. Mirkiani, A. Ghasemi, M. Hoseini-Ghahfarokhi, N. Mozaffari, M. Karimi, M. R. Hamblin, *Chemistry-Select* **2020**, *5*, 10200–10219.
[25] L. Wu, M. Zhang, W. Xu, Y. Dong, *New. Carbon. Mater.* **2022**, *37*, 827–851.
[26] Z. Wang, M. Zhang, W. Ma, J. Zhu, W. Song, *Small* **2021**, *17*, 2100219.
[27] B. Yin, S. Zhang, K. Ke, T. Xiong, Y. Wang, B. K. D. Lim, W. S. V. Lee, Z. Wang, J. Xue, *Nanoscale* **2019**, *11*, 19723–19728.
[28] D. D. Xu, C. X. Xuan, X. Y. Li, Z. B. Luo, Z. Wang, T. Tang, J. F. Wen, M. Li, J. R. Xiao, *Electrochim. Acta* **2020**, *339*, 135912.
[29] Y. Mansourpanah, *Sep. Purif. Technol.* **2022**, *289*, 120777.
[30] Y. W. Li, W. H. Xu, T. Sun, J. H. Yao, *J. Electroanal. Chem.* **2023**, *937*, 117416.
[31] J. Zheng, Y. Zhang, T. Hu, T. Lv, C. Meng, *Crystal Growth Des.* **2018**, *18*, 5365–5376.
[32] Q. Wang, Y. Zhang, H. Jiang, X. Li, Y. Cheng, C. Meng, *Chem. Eng. J.* **2019**, *362*, 818–829.
[33] L. F. Shen, Y. Wang, H. F. Lv, S. Q. Chen, P. A. van Aken, X. J. Wu, J. Maier, Y. Yu, *Adv. Mater.* **2018**, *30*, 1804378.
[34] Y. Kim, Y. Park, M. Kim, J. Lee, K. J. Kim, J. W. Choi, *Nat. Commun.* **2022**, *13*, 2371.
[35] D. Zhao, X. Wang, W. Zhang, Y. Zhang, Y. Lei, X. Huang, Q. Zhu, J. Liu, *Adv. Funct. Mater.* **2023**, *33*, 2211412.

Manuscript received: January 24, 2024
Revised manuscript received: February 17, 2024
Accepted manuscript online: February 22, 2024
Version of record online: March 11, 2024